STIFFNESS AND PROGRESSIVE FAILURE PREDICTION OF 2-D TRI-AXIALLY BRAIDED COMPOSITES

by

Hongyue SHI[a], Haibin LI[a*], Yanchao SHI[b], and Weijie WANG[c]

[a] College of Science, Inner Mongolia University of Technology, Hohhot, China
[b] Inner Mongolia Synthetic Chemical Institute, Hohhot, China
[c] Hohhot Land and Space Planning Institute, Hohhot, China

Original scientific paper
https://doi.org/10.2298/TSCI2403323S

This paper studies the mechanical properties of the 2-D tri-axial braided composite. A volume element is established, so that the classical laminate plate theory and the series-parallel model can be adopted to study a bi-directional stress--strain response. Failure criteria are given and the failure strength is determined. The finite element simulation is used to verify the reliability of the present theoretical model.

Key words: *textile composites, analytical modeling, mechanical properties, damage mechanics, strength*

Introduction

Glass fibers, carbon fibers, and acrylonitrile fibers are widely used for fiber reinforced composites by a winding or braiding molding process, the mother materials include mainly epoxy resin. Compared with metal materials (such as steel, aluminum alloy, *etc.*), the fiber reinforced composites have the advantages in high specific stiffness, high specific strength and designability. After the in-depth development in the Second World War, 2-D and 3-D braided composites have been widely used in aviation, navigation, sports, medical and other fields. The 2-D tri-axial braided composite material is composed of three fiber bundles interwoven, including the fiber bundle in the braided direction (the axial fiber bundle with an angle of 0°), and the offset fiber bundle with an angle of $\pm\theta$°.

There are various approaches to the analysis of the mechanical properties and progressive failure of the braided composites, for examples, the experimental testing and the finite element simulation, and much achievement was obtained. However, experiments always cost much time and high money, while the numerical method requires much efforts in programming and huge computation time, these shortcomings have hindered many practical applications, and many researchers have to find an alternative approach. Now it is widely used to find an equivalent stiffness of braided composites by combining the numerical simulation with mechanical and geometric parameters.

Liu *et al.* [1] suggested an elastoplastic mechanical-thermal model for 2-D tri-axially braided composites, Wei *et al.* [2] adopted a machine learning-based method for short fiber-reinforced composites, Shokrieh and Mazloomi [3] recommended an analytical method for calculating stiffness of 2-D tri-axial braided composites, Cater *et al.* [4] divided braided com-

* Corresponding author, e-mail: lhb@imut.edu.cn

posites into different subunits to capture out-of-plane deformation and predict the elastic modulus of the materials, Deng *et al.* [5] realized bi-directional coupling of scales through top-down homogenization and decomposition process, effectively simulating the stiffness and failure behavior of 2-D tri-axial braided composites. Dang *et al.* [6-8] used the laminate theory to establish the stress-strain response relationship of braided composites and predict the failure process.

At present, there were little literature on strength prediction and progressive failure prediction of braided composites, especially on 2-D tri-axial braided composites with small fiber volume fraction. Due to the inherent complexity of its mesoscale structure, the stiffness matrix of its mother material matrix and the fluctuation of axial fibers have to be considered. In this paper, a bi-directional reversible mapping relationship is established between the global stress-strain response in the volume element level and the local stress-strain response in the fiber bundle level for 2-D tri-axial braided composites. The equivalent thin layer elements are superimposed to form the laminated plate element, and then combine into the representative volume element. The global and local stiffness matrices can be finally obtained, and the progressive failure prediction can be carried out for the braided materials.

Theoretical development

Figures 1(a) and 1(b) show the top view and side view, respectively, of the 2-D tri-axial braided composite representing the volume element. Obviously, the 2-D tri-axial braided composite structure, as shown in fig. 1(d), can be obtained by repeating the representative volume element.

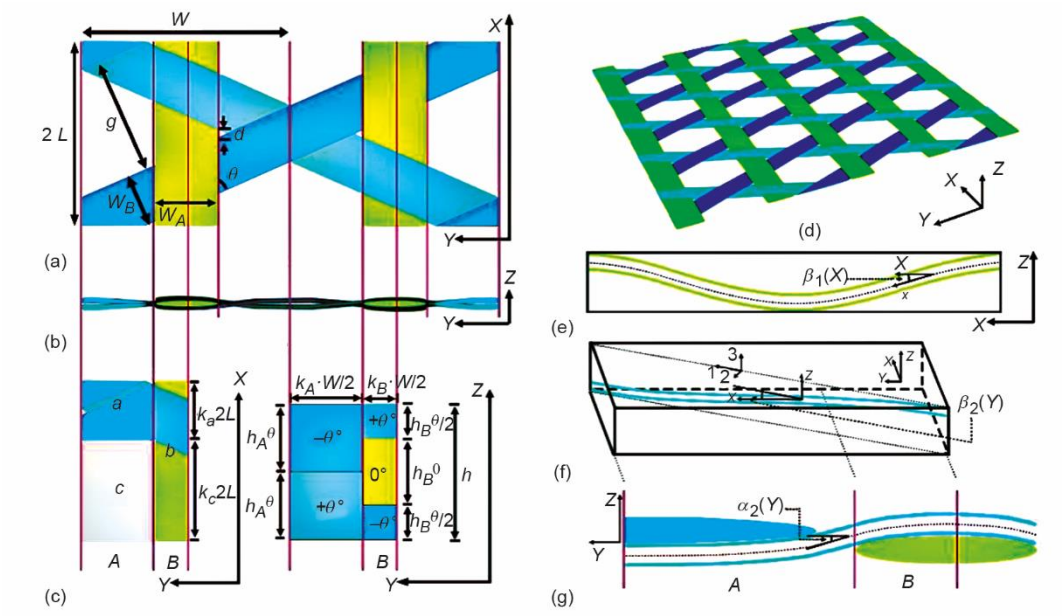

Figure 1. The 2-D tri-axial braided composite; (a) the volume element top view, (b) the volume element side view, (c) geometric dimensions of cells A and B, (d) geometric model of tri-axially braided fabric, (e) undulation of axial fiber bundle in the co-ordinate systems, (f) undulation of bias fiber bundle in the co-ordinate systems, and (g) undulation of the bias fiber bundle in the YZ plane

According to its structural symmetry, the representing volume unit is quartered in the axial direction, as shown in fig. 1(c). This part of the structure can be divided again into the unit A without axial fibers and the unit B with axial fibers. Due to the thickness of 2-D tri-axial braided composites, twisting deformation will occur during stretching, but Cater *et al.* [4] believed that this effect can be basically ignored. Therefore, it can be considered that the stiffness of the quarter cell structure composed of elements A and B can represent the stiffness of the whole representative volume element, which is convenient for the division of elements A and B in the next step. The subunit A is divided into two equivalent thin-layered units $(-\theta°)/(\theta°)$ in the direction of thickness after the subunit *a* is divided into subunit *c* containing only matrix in the axial direction. Similarly, unit B, or subunit *b*, can be approximated as a three-layer equivalent thin-layered element $(\theta°/0°/-\theta°)$. The division of equivalent thin layering units is shown in fig. 1(c).

Based on the classical laminated plate theory [9] for the thickness direction and the series-parallel model of in-plane direction, the mentioned partition process can be backward traced to obtain the equivalent stiffness of the representative volume element.

According to the previous analysis, according to the symmetry, the structural mechanical properties of one quarter composed of elements A and B can represent the mechanical properties of the whole representative volume element. The geometric division and stiffness reassembly are shown in fig. 2. The equivalent stiffness of the fiber bundle in the global co-ordinate system needs to be determined after two co-ordinate transformations.

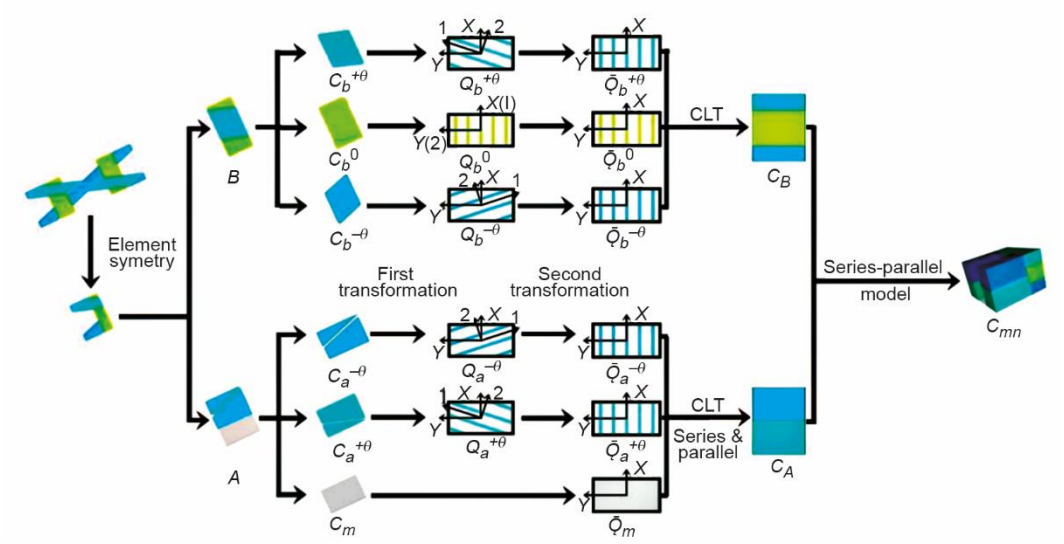

Figure 2. Scheme of geometric division and stiffness reassembly for representative volume element

Local co-ordinates (123) are used to describe the wavy fluctuation of the fiber bundle, as shown in figs. 1(e) and 1(f). Four elastic constants, E_{xx}, E_{yy}, G_{xy}, and v_{xy} can be used to determine the stiffness matrix of the fiber bundle in local co-ordinate (123), as shown in eq. (1). The stiffness matrix of element *c* of the element *A* is expressed by the elastic modulus, E_m, shear modulus, G_m, and Poisson's ratio, v_m, in the form of eq. (2):

$$\left[C_i^j\right]=\left[S_i^j\right]^{-1}=\begin{bmatrix}\dfrac{1}{E_{xx}} & -\dfrac{\nu_{yx}}{E_{yy}} & 0\\ 0 & \dfrac{1}{E_{yy}} & 0\\ \text{symmetric} & 0 & \dfrac{1}{G_{xy}}\end{bmatrix},\quad \begin{cases} i=a & j=-\theta,+\theta \\ i=b & j=+\theta,0,-\theta \end{cases} \tag{1}$$

$$\left[C_m\right]=\begin{bmatrix}\dfrac{1}{E_m} & -\dfrac{\nu_m}{E_m} & 0\\ -\dfrac{\nu_m}{E_m} & \dfrac{1}{E_m} & 0\\ 0 & 0 & \dfrac{1}{G_m}\end{bmatrix}^{-1} \tag{2}$$

The 0° fiber is projected onto the XZ plane, as shown in fig. 1(e). The median line of projection fluctuation is described by Z_1, *i.e.*, eq. (3). The offset fiber is projected onto the YZ plane, as shown in fig. 1(f), and the median of its projection fluctuation is described by Z_2, *i. e.*, eq. (4):

$$Z_1=\frac{h_B^\theta}{2}\cos\left(\frac{X}{L}\pi\right) \tag{3}$$

$$Z_2=\frac{h_i^j}{2}\cos\left(\frac{2Y}{W}\pi\right) \tag{4}$$

where $j=\theta$ when $i=A$ and $j=0$ when $i=B$.

The actual fluctuation angle of Z_1 is equal to the projection angle, and the angle between the plane of the actual fluctuation midline of Z_2 and the plane of the projection fluctuation midline is θ, so we have:

$$\tan\beta_1(X)=\frac{\mathrm{d}Z_1}{\mathrm{d}X}=\frac{\pi h_B^\theta}{2L}\sin\left(\frac{X}{L}\pi\right) \tag{5}$$

$$\begin{aligned}\tan\beta_2(Y)=\tan\alpha_2(Y)\sin(\theta)=\frac{\mathrm{d}Z_2}{\mathrm{d}Y}\sin(\theta)=\\ =\frac{\pi h_i^j}{W}\sin\left(\frac{2Y}{W}\pi\right)\sin(\theta),\quad \begin{cases} i=A,\ j=\theta \\ i=B,\ j=0 \end{cases}\end{aligned} \tag{6}$$

After the actual fluctuation angle of the fiber bundle is obtained, the stiffness matrix is calculated after the first co-ordinate transformation:

$$[Q_b^0] = \int_{\frac{L}{2}}^{\frac{5L}{2}} \frac{[R_1][C_b^0][R_1]^T \mathrm{d}x}{2L}$$

$$[Q_a^j] = \int_0^{\frac{W-W_A}{2}} \frac{[R_2][C_a^0][R_2]^T \mathrm{d}Y}{\frac{W-W_A}{2}}, \quad j = -\theta, +\theta$$

$$[Q_b^j] = \int_{\frac{W-W_A}{2}}^{\frac{w}{2}} \frac{[R_2][C_b^j][R_2]^T \mathrm{d}Y}{\frac{W_A}{2}} \tag{7}$$

where

$$[R_i] = \begin{bmatrix} m_i^2 & 0 & 0 \\ 0 & 1 & 0 \\ 0 & 0 & m_i \end{bmatrix}, \quad i = 1, 2 \tag{8}$$

where

$$m_1 = \frac{1}{\sqrt{1+\tan^2\beta_1(X)}}, m_2 = \frac{1}{\sqrt{1+\tan^2\beta_2(Y)}}, \tan\beta_1(X), \text{ and } \tan\beta_2(Y)$$

are calculated according to eqs. (5) and (6), respectively.

Convert the prevous stiffness matrix into the equivalent stiffness matrix under the following global co-ordinates:

$$\begin{gathered} \left[\bar{Q}_b^0\right] = \left[Q_b^0\right] \\ \left[\bar{Q}_i^j\right] = \left[R_3\right]\left[Q_i^j\right]\left[R_3\right]^T, \quad i = a, b, \; j = -\theta, +\theta \end{gathered} \tag{9}$$

where

$$\left[R_3\right] = \begin{bmatrix} p^2 & q^2 & -2pq \\ q^2 & p^2 & 2pq \\ pq & -pq & p^2 - q^2 \end{bmatrix}, \quad p = \cos(\theta), \quad q = \sin(\theta) \tag{10}$$

The stress-strain relationship of sub-elements *a*, *b*, and *c* can be written:

$$\left[\sigma_X^i \;\; \sigma_Y^i \;\; \sigma_{XY}^i\right]^T = \frac{1}{h}\left[N_X^i \;\; N_Y^i \;\; N_{XY}^i\right]^T = \left[C_i\right]\left[\varepsilon_X^i \;\; \varepsilon_Y^i \;\; \gamma_{XY}^i\right]^T, \quad i = a, b, c \tag{11}$$

where $[C_c] = [C_m]\,[C_a]$ and $[C_b]$ can be obtained from eq. (9) and the laminates theory [10]:

$$\begin{gathered}\left[C_a\right]=\frac{\left[\bar{Q}_a^{+\theta}\right]h_A^{\theta}+\left[\bar{Q}_a^{-\theta}\right]h_A^{\theta}}{h}\\ \left[C_b\right]=\frac{\left[\bar{Q}_b^{+\theta}\right]\frac{h_B^{\theta}}{2}+\left[\bar{Q}_b^{0}\right]h_B^{0}+\left[\bar{Q}_b^{-\theta}\right]\frac{h_B^{\theta}}{2}}{h}=\left[C_B\right]\end{gathered}\tag{12}$$

Based on the series-parallel model [11], it can be assumed that the stress and strain responses in plane *a* and plane *c* of the sub-element have the following six relations:

$$\sigma_X^a=\sigma_X^c=\sigma_X^A,\quad \varepsilon_Y^a=\varepsilon_X^c=\varepsilon_X^A,\quad \sigma_{XY}^a=\sigma_{XY}^c=\sigma_{XY}^A \tag{13}$$

$$k_a\sigma_Y^a+k_c\sigma_Y^c=\sigma_X^A,\quad k_a\varepsilon_X^a+k_c\varepsilon_X^c=\varepsilon_X^A,\quad k_a\sigma_{XY}^a+k_c\sigma_{XY}^c=\sigma_{XY}^A \tag{14}$$

where k_a and k_c are length coefficients in the *X*-direction, see fig. 1(c). The equivalent stiffness matrix of the element A (C^A_{mn}, m, n = 1, 2, 6) can be obtained:

$$\begin{gathered}C_{11}^A=\frac{C_{11}^aC_{11}^c}{k_aC_{11}^c+k_cC_{11}^a}\\ C_{12}^A=\frac{k_aC_{12}^aC_{11}^c+k_cC_{12}^cC_{11}^a}{k_aC_{11}^c+k_cC_{11}^a}\\ C_{21}^A=\frac{k_aC_{21}^aC_{11}^c+k_cC_{21}^cC_{11}^a}{k_aC_{11}^c+k_cC_{11}^a}\\ C_{22}^A=k_aC_{22}^a+k_cC_{22}^c+k_ak_c(C_{21}^a-C_{21}^c)(C_{12}^c-C_{12}^a)\\ C_{66}^A=\frac{C_{66}^aC_{66}^c}{k_aC_{66}^c+k_cC_{66}^a}\end{gathered}\tag{15}$$

Furthermore, the strain components of the sub-element *a* and the sub-element *c* can also be solved, which read:

$$\begin{gathered}\varepsilon_X^a=\frac{C_{11}^c}{k_aC_{11}^c+k_cC_{11}^a}\varepsilon_X^A+\frac{k_c(C_{12}^c-C_{12}^a)}{k_aC_{11}^c+k_cC_{11}^a}\varepsilon_Y^A\\ \varepsilon_X^c=\frac{C_{11}^a}{k_aC_{11}^c+k_cC_{11}^a}\varepsilon_X^A+\frac{k_a(C_{12}^a-C_{12}^c)}{k_aC_{11}^c+k_cC_{11}^a}\varepsilon_Y^A\\ \varepsilon_Y^a=\varepsilon_Y^c=\varepsilon_Y^A\\ \gamma_{XY}^a=\frac{C_{66}^c}{k_aC_{66}^c+k_cC_{66}^a}\gamma_{XY}^A\\ \gamma_{XY}^c=\frac{C_{66}^a}{k_aC_{66}^c+k_cC_{66}^a}\gamma_{XY}^A\end{gathered}\tag{16}$$

The stiffness matrix C_A of the element A can be obtained, and the stiffness matrix of the element B is given in eq. (12), using the series-parallel method, the effective stiffness matrix of the single element (C_{mn}, m, n = 1, 2, 6) can be finally obtained:

$$\begin{aligned} C_{11} &= k_A C_{11}^A + k_B C_{11}^B + k_A k_B (C_{12}^A - C_{12}^B)(C_{21}^B - C_{21}^A) \\ C_{12} &= \frac{k_A C_{12}^A C_{22}^B + k_B C_{12}^B C_{22}^A}{k_A C_{22}^B + k_B C_{22}^A} \\ C_{21} &= \frac{k_A C_{21}^A C_{22}^B + k_B C_{21}^B C_{22}^A}{k_A C_{22}^B + k_B C_{22}^A} \\ C_{22} &= \frac{C_{22}^A C_{22}^B}{k_A C_{22}^B + k_B C_{22}^A} \\ C_{66} &= \frac{C_{66}^A C_{66}^B}{k_A C_{66}^B + k_B C_{66}^A} \end{aligned} \tag{17}$$

Components of strain in elements A and B are:

$$\begin{aligned} \varepsilon_X^A &= \varepsilon_X^B = \varepsilon_X \\ \varepsilon_X^A &= \frac{k_B (C_{21}^B - C_{21}^A)}{k_A C_{22}^B + k_B C_{22}^A} \varepsilon_X + \frac{C_{22}^B}{k_A C_{22}^B + k_B C_{22}^A} \varepsilon_Y \\ \varepsilon_X^B &= \frac{k_A (C_{21}^A - C_{21}^B)}{k_A C_{22}^B + k_B C_{22}^A} \varepsilon_X + \frac{C_{22}^A}{k_A C_{22}^B + k_B C_{22}^A} \varepsilon_Y \\ \gamma_{XY}^A &= \frac{C_{66}^B}{k_a C_{66}^B + k_c C_{66}^A} \gamma_{XY} \\ \gamma_{XY}^B &= \frac{C_{66}^A}{k_a C_{66}^B + k_c C_{66}^A} \gamma_{XY} \end{aligned} \tag{18}$$

where k_A and k_B are width coefficients in the Y-direction.

Using the failure criterion of composite materials, the local stiffness of the equivalent thin layer element should be determined. The laminate theory and the series and parallel model can be used to find the equivalent stiffness for strength prediction.

It is necessary to determine the local stress components in the equivalent thin layup element in the failure criterion. Considering the external load [N_X, N_Y, N_{XY}] acting on the element, the strain can be given by:

$$[\varepsilon_X \quad \varepsilon_Y \quad \gamma_{YY}]^T = \frac{1}{h}[C_{mn}]^{-1}[N_X \quad N_Y \quad N_{YY}]^T, \quad \begin{cases} m = 1,2,6 \\ n = 1,2,6 \end{cases} \tag{19}$$

By using eqs. (18) and (16) in turn, the strain components of sub-elements a, b, and c can be obtained. The stress component of sub-element c is determined by eq. (11), and the local stress of equivalent thin layup element can be given by:

$$[\sigma_1^i \quad \sigma_2^i \quad \tau_{12}^i]^T = [R_3]^{-1}[\bar{Q}_i^j][\varepsilon_X^i \quad \varepsilon_Y^i \quad \gamma_{XY}^i]^T, \quad \begin{cases} i = a, & j = -\theta, +\theta \\ i = b, & j = +\theta, 0, -\theta \end{cases} \tag{20}$$

where [R_3] is determined by eq. (10).

The failure of the sub-element *c* is determined by the maximum stress criterion. The local stress of the equivalent thin layered element is substituted into the following Huffman [12] failure criterion to determine the initial and progress of the fiber bundle failure during loading:

$$f(\sigma_{ij}) = \frac{\sigma_1^2}{X_t X_c} - \frac{\sigma_1 \sigma_2}{X_t X_c} + \frac{\sigma_2^2}{Y_t Y_c} + \frac{X_c - X_t}{X_t X_c}\sigma_1 + \frac{Y_c - X_t}{Y_t Y_c}\sigma_2 + \frac{\tau_{12}^2}{S^2} \tag{21}$$

An iteration program is developed using some a mathematics software and incorporating the above obtained model to simulate the progressive failure process of 2-D tri-axial braided composites.

The local stress is substituted into the failure criterion. If $f(\sigma_{ij}) < 1$, no failure occurs and stiffness does not decrease. Now the load increases to $\sigma_X = \sigma_X \pm \Delta\sigma_X$ or $\sigma_Y = \sigma_Y \pm \Delta\sigma_Y$ for the next iteration, if $f(\sigma_{ij}) \geq 1$, we adopt stress intensity ratios [13]: σ_1^2/X_tX_c, σ_2^2/X_tX_c, and τ_{12}^2/S_{12}^2, and find to find the maximum ratio among them, so that the corresponding equivalent thin layer element failure model can be determined, and the corresponding local stiffness can be selected according to the failure mode. For example, we set $E_{22} = 0$ and $G_{12} = 0$, and E_{22} keeps unchanged, if σ_2^2/Y_tY_c or τ_{12}^2/S_{12}^2 reaches it's maximum, tensile failure, or compression failure, or shear failure occurs in the matrix [14]. This means that the matrix is broken while the fiber bundle can still withstand the load. Now we consider another example when $E_{11} = 0$, $E_{22} = 0$, and $G_{12} = 0$, if σ_1^2/X_tX_c reaches the maximum, this implies that the tensile failure or compression failure in the fiber bundle occurs, and the equivalent element becomes totally damaged, and can not withstand any loads [14].

The damage leads to stiffness degradation, which will change the overall stiffness matrix of sub-elements and elements and the stress distribution. So it is now necessary to check whether the material completely fails at the current loading level. If it fails, the corresponding strength is recorded as the failure strength. Otherwise, an additional external load is acted $\sigma_X = \sigma_X + \Delta\sigma_X$ or $\sigma_Y = \sigma_Y + \Delta\sigma_Y$, and proceed the next iteration.

Finite element model and the mechanical parameters

Finite element (FE) simulation is used to verify the validity of the proposed model. We take a (0°)/(±72°) 2-D braided composite as a sample, which is made of T700s carbon fibers with axial fiber bundle 24 K (0°) and offset fiber bundles 12 K (±72°), and E862 epoxy resin. The axial modulus and transverse modulus of T700s carbon fiber are 230 GPa and 15 GPa, respectively, and the tensile and compressive strength of fiber are 4900 MPa and 2400 MPa, respectively [15]. The E862 epoxy resin is isotropic, with Young's modulus of 2.7 GPa, shear modulus of 1 GPa, tensile, compressive and shear strength of 61 MPa, 92 MPa, and 45 MPa, respectively [16].

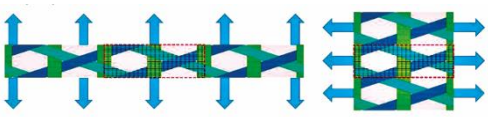

Figure 3. Representative volume element under axial tension and transverse tension

The TEXGEN software, is used to establish the 3-D model of 2-D tri-axial braided composites, and the solid element (C3D8R) is used for discretization. As shown in fig. 3, due to the periodicity of the 2-D tri-axial braided composite and to impose more boundary conditions on the fiber bundle during loading, the finite element cell model is horizontally translated by a quarter of the width of the cell (W/2).

As shown in fig. 1(a), the distance between the two adjacent axial fiber bundles is W, the unit cell has a width of $2W$ and a length of $2L$: $L = W/\tan(\theta)$. The width of 0° fiber bundle is W_A, and W_B for θ° fiber bundles with an angle of δ and the gap: $g = W_B + 2W_A\cos(\theta) + 2\delta\sin(\theta)$. So we have $W = W_B/\cos(\theta) + W_A + \delta\tan(\theta)$, where h^{θ}_A, h^{0}_B, and h^{θ}_B are the equivalent thin bedding element thickness for θ° in cell A, 0° in cell B, and θ° in cell B, respectively.

Based on the above geometric analysis, the equivalent fiber volume fraction of each subunit is:

$$V_a^{\theta} = \frac{\pi d^2 N_{fb}\tan(\theta)}{4h_A^{\theta}(W - W_A)^2}\sqrt{(W - W_A)^2(h_A^{\theta} + h_B^{\theta})^2} \tag{22}$$

$$V_b^{\theta} = \frac{\pi d^2 N_{fb}}{4h_B^{\theta} L\sin(\theta)} \tag{23}$$

$$V_b^{0} = \frac{\pi d^2 N_{fb}}{4h_B^{0} W_A L}\sqrt{(L^2 + h_B^{\theta})^2} \tag{24}$$

where d is the fiber diameter, N_{fa} and N_{fb} are the fiber numbers in axial direction and offset direction, respectively. The composite's geometrical parameter of equivalent thin layer are listed in tab. 1.

Table 1. Geometric characteristics of 2-D tri-axially braided composites

Parameter	Value	Parameter	Value	Parameter [%]	Value
θ [°]	72	h [mm]	0.560	V_a^{θ}	41.34
W [mm]	18.446	h_A^{θ} [mm]	0.280	V_b^{θ}	31.15
W_A [mm]	3.30	h_B^{θ} [mm]	0.260	V_b^{0}	56.00
W_B [mm]	3.50	h_B^{0} [mm]	0.300	$V_b^{-\theta}$	31.15
L [mm]	5.993	$V_a^{-\theta}$ [%]	41.34	–	–

The Chamis model [17] is used to determine the four elastic parameters (E_{xx}, E_{yy}, G_{xy}, and v_{xy}), and five strength parameters (X_t, X_c, Y_t, Y_c, and S) of the equivalent thin-layed ele-ment of the micromodel. Elastic parameters and strength are listed in tab. 2. The compressive strength is calculated using the approach given in [18], which determines the compressive strength as the average of the three possible failure modes considered in the Chamis model (fiber fracture, buckling, and delamination).

Results and discussion

In this section, the analysis model is verified by the finite element simulation. The equivalent stiffness, stress-strain curve, and progressive failure behaviors are analyzed.

The predicted stiffness is compared with that by the finite element simulation, see tab. 3, seeing a relatively good agreement, the errors might arise in the composite thickness, which is not considered in our model.

Table 2. Elastic moduli and strength of equivalent thin layer

Equivalent thin layer	E_{xx} [GPa]	E_{yy} [GPa]	G_{xy} [GPa]	v_{xy}	X_t [MPa]	X_c [MPa]	Y_t [MPa]	Y_c [MPa]	S [MPa]
a-72°	96.7	5.7	2.6	0.33	2026	1051	49.5	74.7	35.1
a-72°	96.7	5.7	2.6	0.33	2026	1051	49.5	74.7	35.1
b-72°	73.5	5.0	2.1	0.33	1526	890	48.7	73.4	34.4
b-0°	130.0	7.0	3.5	0.32	2744	1341	51.6	77.8	36.9
b-72°	73.5	5.0	2.1	0.33	1526	890	48.7	73.4	34.4

Table 3. Analytical results on stiffness

Methods	E_{xx} [GPa]	E_{yy} [GPa]
FE	22.3	26.6
Prediction	23.5	28.1

The predicted strength is compared with that by the finite element simulation under axial and transverse tensile conditions, see fig. 4 and tab. 4.

Table 4. Strength and failure strain under various loading conditions

Methods		Strength [MPa]	Strain [%]	Methods		Strength [MPa]	Strain [%]
Axial	FE	354	1.81	Transverse	FE	376	1.58
tension	Analytical	375	1.84	tension	Analytical	428	1.58

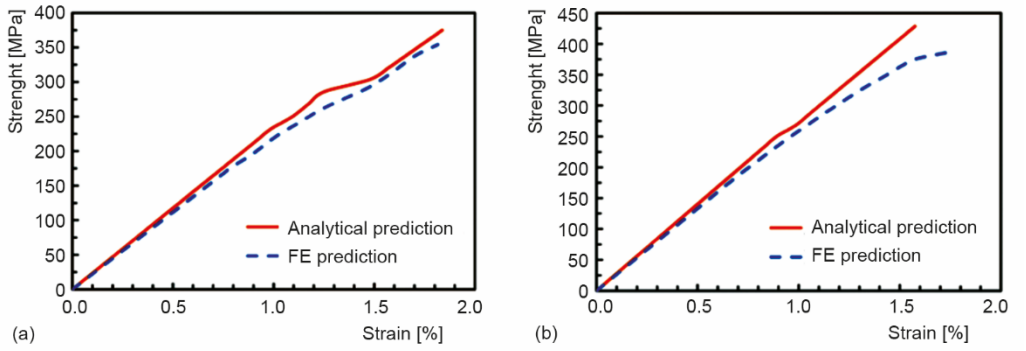

Figure 4. Stress-strain curves under different loading condition; (a) axial tension and (b) transverse tension

It can be seen from fig. 4 that the stress-strain curves of our strength prediction sees a good agreement with that by the finite element simulation for the initial stiffness for both cases of axial and transverse tensile stresses. Due to the use of plane stress hypothesis ($\sigma_3 = \tau_{13} = \tau_{23} = 0$), our strength model has limitations of three dimensional prediction, however the relatively error is less than 14% in our prediction.

The progressive failure process under axial and lateral loading conditions is compared with that by the finite element simulation, see fig. 5.

Under axial tensile load, it is predicted that the matrix tensile failure occurs first in the ±72° equivalent thin bedding element in element B, followed by the matrix tensile failure in the ±72° equivalent thin bedding element in element A and the 0° equivalent thin bedding element in element B. Finally, the fiber tensile failure occurs in the 0° equivalent thin bedding element in element B. In the finite element results, the strain level corresponding to the failure of ±72° equivalent thin-layed element is consistent with our prediction, and the failure of 0° equivalent thin-layed element matrix occurs earlier, which also leads to a 5.4% difference in stiffness prediction.

Under the transverse tensile load, it is predicted that the tensile failure of the matrix first occurs on the 0° fiber of element B, then on the ±72° equivalent thin layup element of element A, and finally on the 0° equivalent thin layup element of element B. In the finite element analysis, the axial fibers first suffer tensile failure of matrix, and then the final failure is caused by the failure of offset fibers.

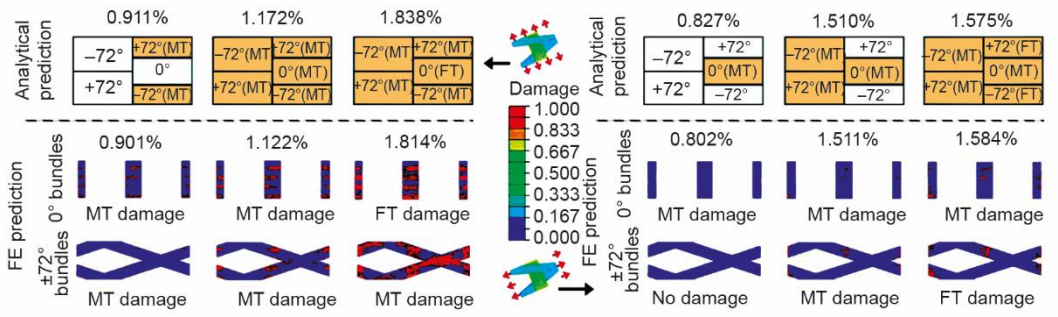

Figure 5. Progressive failure prediction under axial tension and transverse tension; MT is the tensile failure of the matrix and FT – the tensile failure of the fiber

It can be seen that under axial and transverse tensile loads, the failure modes and strain levels of the proposed model and finite element analysis are consistent in the progressive failure progression.

Conclusions

In this paper, a mechanical model combining laminate theory with series-parallel model is used to simulate the axial and transverse stiffness of 2-D tri-axial braided composites under Chamis model [17]. Then progressive failure and strength analysis are introduced. The results of this paper are compared with those of finite element analysis, and a good agreement is seen.

Since the theory of laminates and the series-parallel model are computationally simple and efficient, the analysis method in this paper can be further extended to other braided composites, providing an efficient algorithm for mechanical simulation in the design of other composites. Further study is to study the effects of electrical-mechanical coupling behaviors [19, 20] and the micro/nano structure [21] on the tri-axial braided composites properties.

Acknowledgment

This research was supported by the National Natural Science Foundation of China (Grant No. 11962021), the Natural Science Foundation of Inner Mongolia (Grant No. 2021MS05020).

References

[1] Liu, P., *et al.*, An Elastoplastic Mechanical-Thermal Model for Temperature Rise Simulation of 2-D Tri-Axially Braided Composites Under Quasi-Static Loads, *Composite Structures*, *306* (2023), 116559
[2] Wei, H. Y., *et al.*, LS-DYNA Machine Learning-Based Multiscale Method for Non-linear Modeling of Short Fiber-Reinforced Composites, *Journal of Engineering Mechanics*, *149* (2023), 3, 04023003
[3] Shokrieh, M. M., Mazloomi, M. S., An Analytical Method for Calculating Stiffness of 2-D Tri-Axial Braided Composites, *Composite Structures*, *92* (2010), 12, pp. 2901-2905
[4] Cater, C. R., *et al.*, Single Ply and Multi-Ply Braided Composite Response Predictions Using Modified Subcell Approach, *Journal of Aerospace Engineering*, *28* (2015), 5, 04014117
[5] Deng, Y., *et al.*, A Multi-Scale Correlating Model for Predicting the Mechanical Properties of Tri-Axial Braided Composites, *Journal of Reinforced Plastics & Composites*, *32* (2013), 24, pp. 1934-1955
[6] Dang, H. Y., *et al.* Theoretical Prediction for Effective Properties and Progressive Failure of Textile Composites: A Generalized Multi-Scale Approach, *Acta Mechanica Sinica*, *37* (2021), 8, pp. 1222-1244
[7] Dang, H. Y., *et al.* A New Analytical Method for Progressive Failure Analysis of 2-D Tri-Axially Braided Composites, *Composites Science and Technology*, *186* (2020), 107936
[8] Dang, H. Y., *et al.*, Progressive Failure Prediction of Three-Dimensional Woven Composites Using a Generic Multi-Scale Analytical Model, *Composite Structure*, *303* (2023), 116321
[9] Saeed, K., *et al.*, Predication of the In-Plane Mechanical Properties of Continuous Carbon Fibre Reinforced 3D Printed Polymer Composites Using Classical Laminated-Plate Theory, *Composite Structures*, *259* (2021), 113226
[10] Potluri, P., *et al*,. Flexural And Torsional Behaviour of Biaxial and Tri-Axial Braided Composite Structures, *Composite Structures*, *75* (2006), 1-4, pp. 377-386
[11] Li, J. J., *et al.* Modeling the Stiffness, Strength, and Progressive Failure Behavior of Woven Fabric-Reinforced Composites, *Journal of Composite Materials*, *48* (2014), 6, pp. 735-747
[12] Hoffman, O., The Brittle Strength of Orthotropic Materials, *Journal of Composite Materials*, *1* (1967), 2, pp. 200-206
[13] Zako, M., *et al.*, Numerical Prediction of Strength of Notched UD Laminates by Analyzing the Propagation of Intra- and Inter-Laminar Damage, *Journal of the Society of Materials Science Japan*, *45* (1996), 6, pp. 117-122
[14] Jing, M., *et al.* Ultimate Strength Prediction of 2-D Tri-Axial Braided Composites Based on an Analytical Laminate Model, *Journal of Reinforced Plastics and Composites*, *37* (2018), 13, pp. 917-929
[15] Oya, N., Johnson, D. J., Longitudinal Compressive Behaviour and Microstructure of PAN-Based Carbon Fibres, *Carbon*, *39* (2001), 5, pp. 635-645
[16] Littell, J., The Experimental and Analytical Characterization of the Macro-Mechanical Response for Tri-Axial Braided Composite Materials, PhD thesis, The University of Akron, Akron, USA, 2008
[17] Chamis, C. C., Simplified composite Micromechanics Equations for Strength, Fracture Toughness and Environmental Effects, *NASA Technical Memorandum*, *15* (1984), 4, pp. 41-55
[18] Li, X., *et al.*, Finite Element Model for Failure Study of Two Dimensional Tri-Axially Braided Composite, *Journal of Aerospace Engineering*, *24* (2010), 2, pp. 170-180
[19] Bai, L., *et al.*, Electrical-Mechanical Coupling Behaviors and Thermal-Resistance Effects of 3D Braided Composites, *Journal of Donghua University* (*English Edition*), *38* (2021), 5, pp. 385-391
[20] Jankowski, P., Detection of Nonlocal Calibration Parameters and Range Interaction for Dynamics of FDM Porous Nanobeams Under Electro-Mechanical Loads, *Facta Universitatis, Series: Mechanical Engineering*, *20* (2022), 3, pp. 457-478
[21] Zhou, H. L., *et al.*, Effects of Microstructure on Quasi-Static Transverse Loading Behavior of 3D Circular Braided Composite Tubes, *Journal of Donghua University* (*English Edition*), *38* (2021), 5, pp. 392-397

Paper submitted: March 10, 2023
Paper revised: August 6, 2023
Paper accepted: August 7, 2023